Amine-Rich Hydrogels Enhance Solar Water Oxidation via Boosting Proton-Coupled Electron Transfer

Sanghyun Bae, Rod Alexei Fitrian De Guzman, Dasom Jeon, Minjung Kim, and Jungki Ryu*

Photoelectrochemical (PEC) water oxidation is a highly challenging task that acts as a bottleneck for efficient solar hydrogen production. It is because each cycle of water oxidation is composed of four proton-coupled electron transfer (PCET) processes and conventional photoanodes and cocatalysts have limited roles in enhancing the charge separation and storage rather than in enhancing catalytic activity. In this study, a simple and generally applicable strategy to improve the PEC performance of water oxidation photoanodes through their modification with polyethyleneimine (PEI) hydrogel is reported. The rich amine groups of PEI not only allow the facile and stable modification of photoanodes by crosslinking but also contribute to improving the kinetics of PEC water oxidation by boosting the PCET. Consequently, the PEC performance of various photoanodes, such as $BiVO_4$, Fe_2O_3, and TiO_2, is significantly enhanced in terms of photocurrent densities and onset potentials even in the presence of notable cocatalyst, cobalt phosphate. The present study provides new insights into and strategies for the design of efficient photoelectrodes and PEC devices.

1. Introduction

Solar water oxidation is one of the most important but challenging electrochemical reactions because it acts as a clean source of electrons and protons for the reductive synthesis of various target chemicals in natural and artificial photosynthesis but also as a bottleneck due to its sluggish kinetics and high overpotential.[1–3] Its multiple proton-coupled electron transfer (PCET) nature also poses significant hurdles for effective solar water oxidation. Each cycle of solar water oxidation is composed of four PCET processes, which often involve the formation of high-energy intermediates and result in sluggish reaction kinetics.[4–7] In particular, the first and second PCET steps for the formation of *OH and *O intermediates often act as the rate-determining step (RDS) of the overall solar water oxidation.[4,5] In each PCET process, three reactions pathways are possible depending on reaction coordinates: proton transfer (PT) followed by electron transfer (ET), ET followed by PT, and concerted proton-electron transfer (CPET). It is reported that the concerted transfer can bypass the high-energy intermediates that are inevitably formed in the sequential counterparts, facilitating the overall reaction.[8–10] In natural photosynthesis, interestingly, researchers found that protic functional moieties such as tyrosine near the oxygen-evolving complex of photosystem II facilitate CPET and enhance solar water oxidation.[10–12]

On the other hand, the CPET has been less explored for solar water oxidation in artificial photosynthesis. To date, most studies in photoelectrochemical (PEC) water oxidation have been focused on developing better light-harvesting materials, more efficient cocatalysts, and surface modification with protection layers for improving stability and overpotentials. For instance, various inorganic and organic semiconductors have been explored as photoanodes, such as WO_3,[13] Fe_2O_3,[14,15] $BiVO_4$,[16,17] organic–inorganic metal halide perovskites,[18] etc., for more effective utilization of sunlight. Additionally, various inorganic water oxidation cocatalysts (WOCs), such as cobalt phosphate (CoPi),[19] (oxy)hydroxides,[17,20] layered double hydroxides (LDH),[21] etc., and metal oxide overlayers have been investigated to improve the reaction kinetics and stability of photoanodes by passivating surface-states, effectively accumulating photogenerated holes, increasing photovoltage, and/or forming protective overlayers.[19–21] In contrast, less attention has been paid to enhancing the reaction kinetics of solar water oxidation by facilitating CPET through the modification with

S. Bae, R. A. F. De Guzman, D. Jeon, M. Kim, J. Ryu
Department of Energy Engineering
School of Energy and Chemical Engineering
Ulsan National Institute of Science and Technology (UNIST)
Ulsan 44919, Republic of Korea
E-mail: jryu@unist.ac.kr
S. Bae, D. Jeon, M. Kim, J. Ryu
Emergent Hydrogen Technology R&D Center
Ulsan National Institute of Science and Technology (UNIST)
Ulsan 44919, Republic of Korea
J. Ryu
Graduate School of Carbon Neutrality
Ulsan National Institute of Science and Technology (UNIST)
Ulsan 44919, Republic of Korea

ADVANCED
SCIENCE NEWS
www.advancedsciencenews.com

ADVANCED
MATERIALS
INTERFACES
www.advmatinterfaces.de
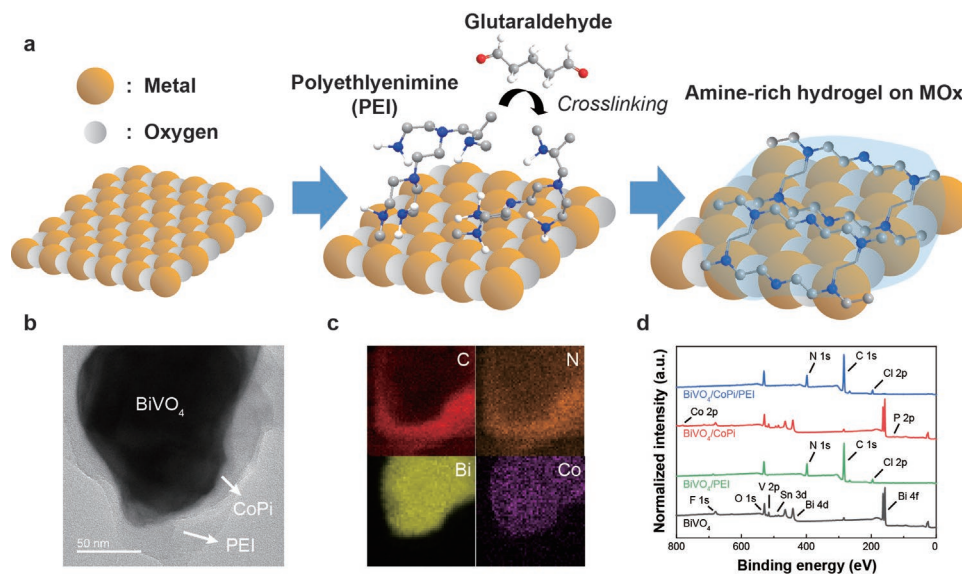
Figure 1. a) Schematic illustrations for the deposition of PEI hydrogel on various metal oxide photoanodes. PEI was spin-coated and then crosslinked via covalent bonding between amine groups using glutaraldehyde. b) TEM and c) elemental mapping analyses of BiVO$_4$/CoPi/PEI. d) XPS spectra of BiVO$_4$-based photoanodes.

organic functional moieties. Although there have recently been a few such attempts based on mimicking the CPET process of photosystem II, these attempts have been limited to the proof-of-concept demonstration. They rely on complex and labile materials and have a limited enhancement effect and poor stability.[10,12,22,23]

Herein, we report a simple method to boost PCET of water oxidation photoanodes by modifying their surface with amine-rich hydrogel. Briefly, amine-rich hydrogel was readily deposited on various photoanodes, such as nanoporous BiVO$_4$, wormlike Fe$_2$O$_3$, and nanotubular TiO$_2$, without altering their inherent properties by spin-coating and crosslinking of polyethyleneimine (PEI). We found that the deposition of PEI hydrogel significantly improves the performance of PEC water oxidation, regardless of types/morphologies of photoanodes and the presence of CoPi cocatalysts. Our analyses by pH-dependent PEC characterization, electrochemical impedance spectroscopy (EIS), and rate law analysis suggest that the PEI modification facilitates the first and second PCET steps for the formation of *OH and *O intermediates, which are frequently considered as the RDS of solar water oxidation. We deduce that protic amine groups of the PEI hydrogel promote the formation of hydroxide ion near the photoanode surface and *OH and *O intermediates, resulting in improved solar water oxidation via CPET. Our study can provide insights into the development of efficient photoanodes and water oxidation cocatalyst by enhancing PCET through hybridization with organic functional materials.
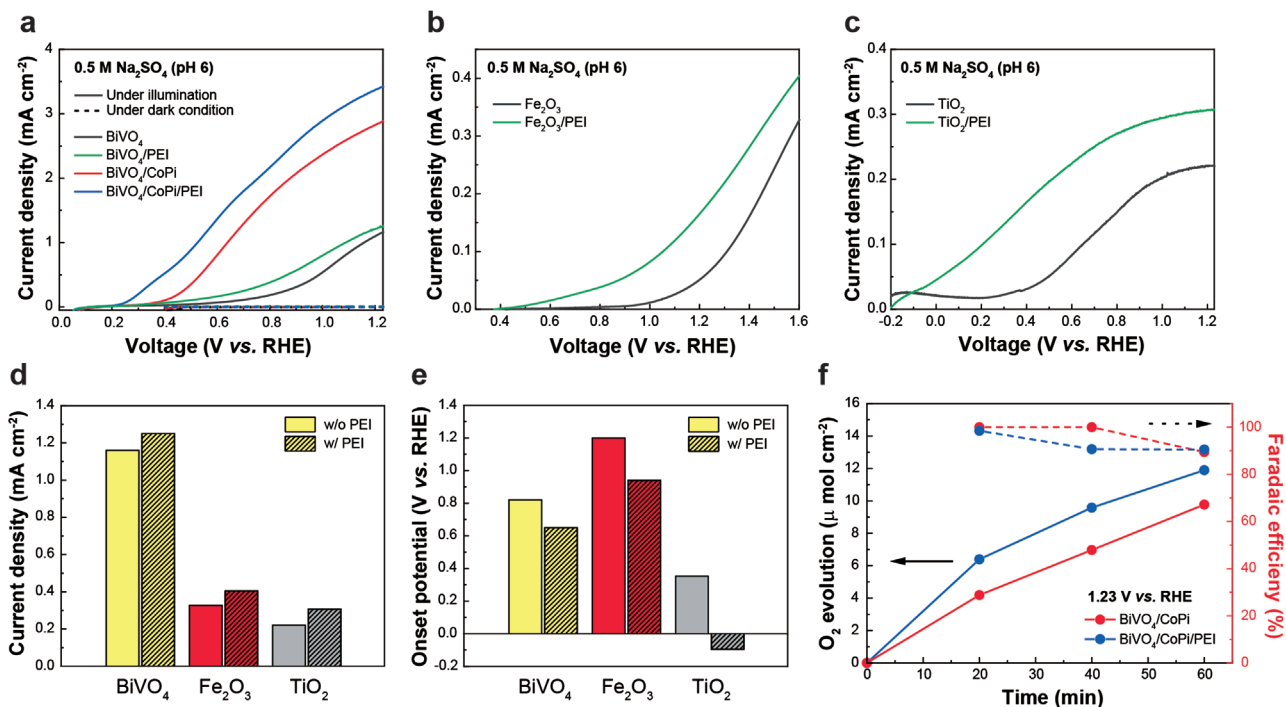
2. Results and Discussion

2.1. Modification of Photoanodes with PEI Hydrogel

Thin PEI hydrogel layer was deposited on various photoanodes with and without cocatalysts by spin-coating followed

by crosslinking (**Figure 1**). Commercially available branched PEI was selected as a model organic modifier of photoanodes because we anticipated that its rich amine groups can promote CPET through their protonation/deprotonation for enhanced solar water oxidation. Additionally, PEI can be readily crosslinked via Schiff-base condensation using glutaraldehyde for improving their stability and adhesion to photoelectrodes (Figure 1a and Figure S1, Supporting Information). Fourier-transform infrared (FT-IR) spectroscopy confirmed the chemical crosslinking of PEI by glutaraldehyde (Figure S2, Supporting Information). To demonstrate our hypothesis that the PEI hydrogel can enhance the PEC performance of water oxidation photoanodes by boosting PCET, we tested three representative photoanodes such as BiVO$_4$,[16,17,24] Fe$_2$O$_3$,[14,15,25] and TiO$_2$.[15,26] Particularly, to validate our approach for practical application, we modified nanoporous BiVO$_4$—that is one of the best photoanodes reported to date—in the presence and absence of notable CoPi cocatalysts (BiVO$_4$/CoPi and BiVO$_4$, respectively) with PEI hydrogel (BiVO$_4$/CoPi/PEI and BiVO$_4$/PEI, respectively). CoPi can be an ideal model cocatalyst to validate our approach because it is known to improve the efficiency of solar water oxidation by enhancing the charge separation and effectively accumulating photogenerated holes rather than enhancing catalytic activity.[16,24,27,28] Despite poor visible-light activity, TiO$_2$ was employed for in-depth analysis because of its excellent electrical properties[5,26] and pH-independent stability.[15]

The formation of thin hydrogel layer on various photoanodes was confirmed by electron microscopy, elemental mapping analysis, and X-ray photoelectron spectroscopy (XPS). Transmission and scanning electron microscopy (TEM and SEM, respectively) confirmed that crosslinked PEI layer was well coated on the entire surface of various photoanodes, such as nanoporous BiVO$_4$ (Figure 1b and Figure S3, Supporting Information), wormlike hierarchically porous Fe$_2$O$_3$

ADVANCED
SCIENCE NEWS

www.advancedsciencenews.com

ADVANCED
MATERIALS
### INTERFACES

www.advmatinterfaces.de

Figure 2. Effect of the deposition of the PEI hydrogel on the PEC performance of various water oxidation photoanodes. LSV curves of a) $BiVO_4$, b) Fe_2O_3, and c) TiO_2 photoanodes. d,e) Comparison of the PEC performance of various photoanodes in terms of d) photocurrent density and e) onset potential at 1.23 V versus RHE under AM 1.5 G illumination. f) PEC O_2 evolution profiles of $BiVO_4$/CoPi with and without PEI.

(Figure S4, Supporting Information), and nanotubular TiO_2 (Figure S5, Supporting Information). According to elemental mapping analysis, ≈40 nm thick PEI hydrogel was quite uniformly coated on the surface of $BiVO_4$ irrespective of the presence of CoPi cocatalysts, forming the photoanode/cocatalyst core and the crosslinked PEI shell (Figure 1c and Figure S6, Supporting Information). The formation of the PEI layer was also confirmed by surface-sensitive XPS. For both $BiVO_4$ and $BiVO_4$/CoPi, strong peaks of Bi 4f and V 2p (and additionally Co 2p and P 2p peaks for $BiVO_4$/CoPi) were detected, implying the non-uniform island growth of CoPi as reported previously (Figure 1d).[29] In contrast, only the strong peaks of O 1s, N 1s, and C 1s from PEI and no peaks from $BiVO_4$ and CoPi were identified for both $BiVO_4$/PEI and $BiVO_4$/CoPi/PEI. Similar results were obtained for wormlike Fe_2O_3 (Figure S7, Supporting Information) and nanotubular TiO_2 (Figure S8, Supporting Information). These results confirm the uniform and complete coverage of the PEI layers on the photoanode surface, regardless of types and morphologies. Note that there was a negligible absorbance change after the deposition of PEI layers due to the inherent transparency of PEI and uniformity of the layers.

2.2. Effect of PEI Hydrogel on PEC Performance

Based on these results, we investigated the effect of the PEI hydrogel layer on the PEC performance of various photoanodes. Linear sweep voltammetry (LSV) was conducted in 0.5 M Na_2SO_4 (pH 6.0) under one sun illumination and dark condition

(**Figure 2** and Figure S9, Supporting Information). The deposition of the crosslinked PEI layer improved both the onset potentials and photocurrent densities of all the tested photoanodes even without cocatalysts (Figure 2a–e and Figure S10, Supporting Information). After the deposition, the onset potentials of $BiVO_4$, Fe_2O_3, and TiO_2 photoanodes for PEC water oxidation were cathodically shifted from 0.81 to 0.66, from 1.20 to 0.95, and from 0.35 to −0.10 V versus reversible hydrogen electrode (RHE), respectively. The corresponding photocurrent densities at 1.23 V versus RHE were increased from 0.926 ± 0.022 to 1.064 ± 0.103, from 0.06 to 0.18, and from 0.22 to 0.31 mA cm⁻². Moreover, we found that such an enhancement effect can be observed even in the presence of CoPi cocatalysts (Figure 2a). As a result, $BiVO_4$/CoPi/PEI showed a huge cathodic shift of the onset potential from 0.81 to 0.23 V versus RHE and threefold increase of photocurrent density compared to the bare $BiVO_4$ (Figure 2a and Figure S11, Supporting Information). According to previous reports,[30,31] there is a possibility that PEI hydrogel facilitates the desorption of oxygen gas by increasing electrode's aerophobicity and improve the PEC performance. Considering that onset potentials cannot be improved by facilitating the gas bubble removal, it is thought that the observed performance is mainly caused by altering reaction kinetics rather than facile bubble removal. Of note, the deposition of a thicker PEI layer (≈80 nm) led to the degradation of performance (Figure S12, Supporting Information) probably due to the non-conducting nature of PEI and increased blocking of the electrode surface, as demonstrated by impedance analysis (Figure S13 and Table S1, Supporting Information).[30,31,32] The Faradaic efficiencies of $BiVO_4$/CoPi and $BiVO_4$/CoPi/PEI (Figure 2f) photoanodes
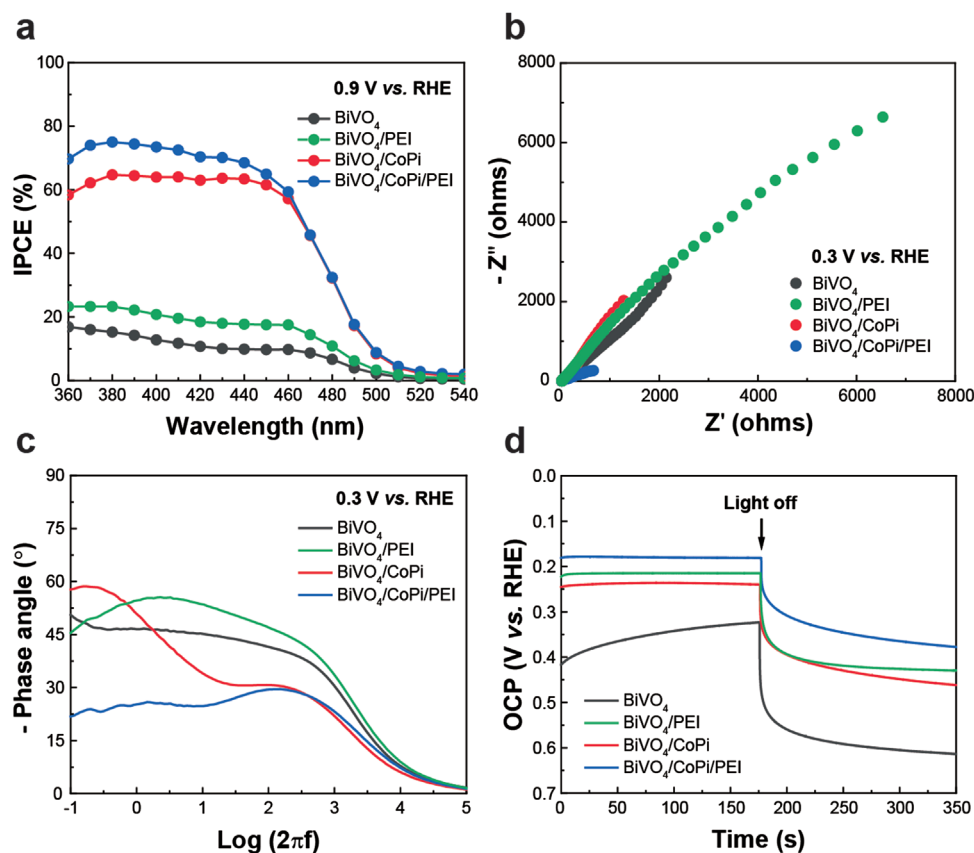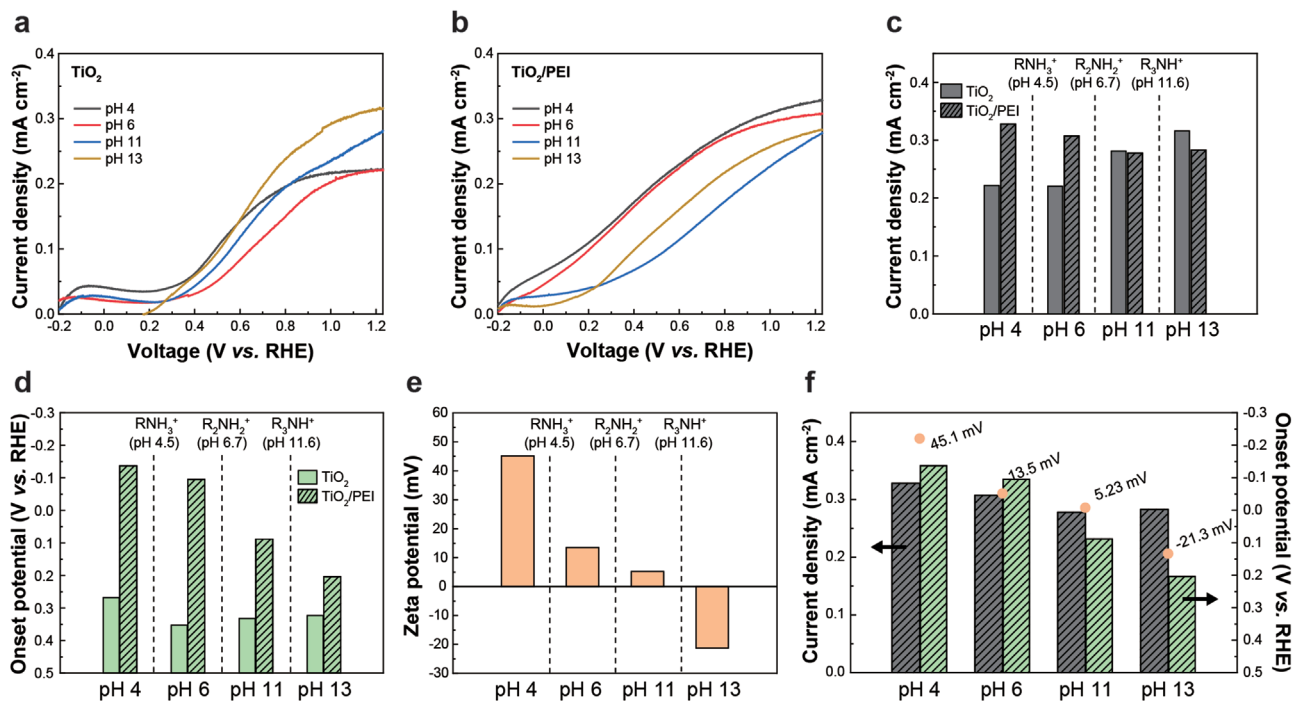
Figure 3. PEC analysis of $BiVO_4$, $BiVO_4$/PEI, $BiVO_4$/CoPi, and $BiVO_4$/CoPi/PEI photoanodes: a) IPCE spectra, b) Nyquist plot analysis, c) Bode plot analysis, and d) OCP measurement.

at 1.23 V versus RHE under light were 90.6% and 90.0%, respectively, excluding the possibility of side reactions by the deposited PEI (Figure S14, Supporting Information). Non-unity faradaic efficiency can be attributed to the photocorrosion of $BiVO_4$, as reported previously.[33,34] Of note, the Faradaic efficiencies were measured in 0.1 M phosphate buffer (pH 6.0) to ensure the stability of CoPi.[17,19,29]

2.3. PEC Analysis

To clarify the role of the PEI layers on the enhanced PEC performance, we conducted incident photon-to-electron conversion efficiency (IPCE) analysis, EIS, and open circuit potential (OCP) measurements. IPCE analysis showed that there was no change in the wavelength-dependent tendency of the IPCE spectra except for the increase of the efficiency after the deposition of CoPi and/or PEI for both $BiVO_4$ and Fe_2O_3 (**Figure 3**a and Figure S15, Supporting Information). These results indicate that the improved PEC performance stems from the enhanced charge separation and/or catalytic charge transfer rather than improved light absorption. EIS analysis of the $BiVO_4$-based photoanodes suggests that the improved performance can be attributed mostly to the enhanced catalytic charge transfer. According to Nyquist plot analysis, the PEI modification lowered the resistance of photoanodes (Figure 3b, Figures S16

and S17a, Supporting Information). In particular, the Bode plot analysis (Figure 3c and Figure S17b, Supporting Information) showed that the PEI modification resulted in a significant blue shift of the low-frequency component, whereas the high-frequency component remained unshifted. Note that the peak frequency of the former and latter can be related to the rate of the catalytic charge transfer at the photoanode–electrolyte interface and that of the charge separation in the bulk photoanode, respectively.[16,20,24] In addition, $BiVO_4$/CoPi/PEI had a much smaller phase angle in the low-frequency region than the other photoanodes, indicating the reduced charge accumulation due to improved catalytic activity. The OCP analysis showed that the quasi-Fermi level of electrons (the OCP value under light) was cathodically shifted after the modification with CoPi and/or PEI (Figure 3d). This result suggests retarded charge recombination of exciton on photoanode surface, which can provide a higher chance of multi-hole reactions for multiple PCET processes.[16,23,35,36] However, considering no or negligible shift of the high-frequency component in the EIS analysis, the improved PEC performance by the deposition of PEI layers might be dominantly affected by the enhanced charge transfer. Since PEI is a non-conducting polymer and is expected to have poor catalytic activity alone, we hypothesize that numerous amine groups of PEI are responsible for the enhanced PEC performance probably by boosting PCET via protonation/deprotonation in solar water oxidation. Kinetic isotope effect (KIE)
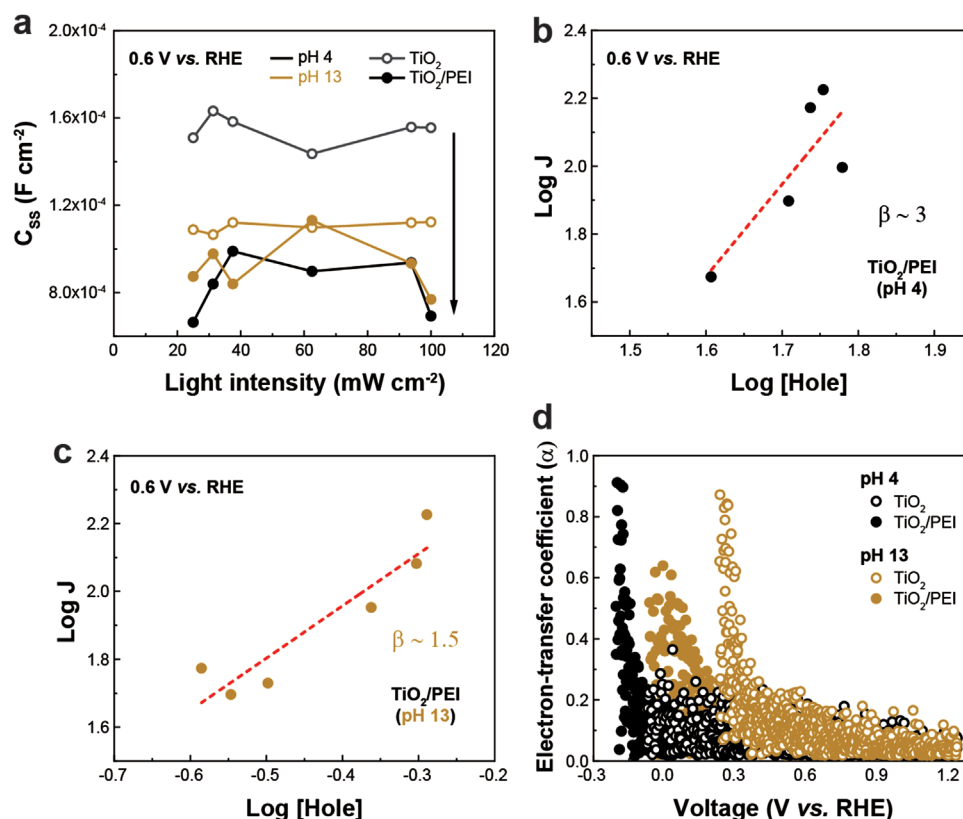
**ADVANCED
SCIENCE NEWS**

www.advancedsciencenews.com

**ADVANCED
MATERIALS
INTERFACES**

www.advmatinterfaces.de

Figure 4. Effect of the pH on the PEC performance and physicochemical properties of the bare TiO_2 and TiO_2/PEI photoanodes under UV illumination. a,b) LSV curves of the corresponding photoanodes. Comparison between PEC performance of the photoanodes with and without the PEI modification at various pHs in terms of c) photocurrent densities at 1.23 V versus RHE and d) onset potentials obtained by the extrapolation at the maximum slope of photocurrent densities. e) pH-dependent zeta potentials of PEI. f) Relationship between the PEC performance of TiO_2/PEI and the zeta potential of PEI.

analysis supports our hypothesis. The PEI modification of $BiVO_4$ led to a significant increase in the KIE values (Figure S18, Supporting Information). According to the literature,[9] these results support the CPET process in water oxidation by improved deprotonation of water molecules by PEI hydrogels.

To further verify our hypothesis, we studied the influence of the pH on the PEC performance of TiO_2 photoanodes with and without the PEI modification under UV illumination (**Figure 4**). TiO_2 was selected due to its excellent stability in the broad pH range from acidic to basic solutions. In addition, its excellent electrical properties[5,26] can minimize the effect of the PEI modification on the charge separation behavior. Bare TiO_2 photoanodes generally exhibited enhanced PEC performance at higher pHs (Figure 4a), whereas TiO_2/PEI exhibited the best PEC performance under acidic conditions in terms of both the onset potential and photocurrent densities (Figure 4b–d). Although TiO_2/PEI allowed slightly lower photocurrent densities than TiO_2 at high pHs, the former had significantly lower (i.e., more cathodic) onset potentials than the latter at all the pHs tested. These results are contrary to the previous reports that most (photo)electrodes including TiO_2 have higher catalytic activity for water oxidation at higher pHs. A high concentration of OH^- under basic conditions can facilitate the formation of the first and second intermediates of water oxidation (i.e., *OH and *O).[4,5,7,37,38] It is anticipated that the pH-dependent protonation of branched PEI plays a pivotal role in the observed tendency of the pH-dependent PEC performance. The pKa values of the primary, secondary, and tertiary amines of PEI are known to be 4.5, 6.7, and 11.6, respectively.[14,39,40] According to our measurement, the zeta potentials of PEI at pH 4.0, 6.0,

11.0, and 13.0 were 45.1, 13.5, 5.23, and −21.3 mV, respectively (Figure 4e). Interestingly, there was a similar tendency between the zeta potential of PEI and the performance improvement by the deposition of PEI, supporting our hypothesis regarding the critical role of the PEI protonation (Figure 4f). Interestingly, the PEI hydrogel modification strategy was also effective even under extremely acidic conditions of 1 M H_2SO_4 (Figure S19, Supporting Information) although there can be stability issues. To check the stability of PEI hydrogel coating, we conducted XPS characterization after chronoamperometry measurement for 1 h (Figures S20 and S21, Supporting Information). In our measurement, the intensity of nitrogen peak from PEI hydrogel was decreased after the reaction but their position was maintained at 400.08 eV. These results can be attributed to the detachment of PEI layers from the photoanode surface, rather than electrochemical degradation of PEI. Further studies are required to improve the stability of the PEI overlayers.

To elucidate the origin of the enhanced PEC water oxidation by the PEI modification, we investigated the charge carrier dynamics of TiO_2 photoanodes with and without the modification by EIS and rate-law analyses. To this end, Nyquist plots were measured at various light intensities and fitted using a two-RC equivalent circuit to determine the surface-state capacitance (Css) related to charge accumulation (**Figure 5**a). The bare TiO_2 and TiO_2/PEI photoanodes had the lowest Css values at pH 13 and pH 4, respectively, and the deposition of PEI lowered the Css values. Considering that a low Css value is an indication of facile charge transfer of the surface-accumulated holes, these results suggest again that the deposition of PEI hydrogel resulted in a significant improvement

ADVANCED
SCIENCE NEWS
www.advancedsciencenews.com

ADVANCED
MATERIALS
INTERFACES
www.advmatinterfaces.de

Figure 5. Kinetic analysis of TiO$_2$ and TiO$_2$/PEI photoanodes by EIS and rate law analyses. a) Light intensity-dependent Css values of the corresponding photoanodes. b,c) Reaction orders for the TiO$_2$/PEI photoanodes at b) pH 4 and c) pH 13. The reaction orders were calculated from EIS data. d) Investigation of the electron-transfer coefficient of the corresponding photoanodes at acidic and basic pHs, where PEI is almost completely protonated and deprotonated, respectively.

of water-oxidation kinetics,[24,28,41] especially at low pHs where most amine groups are protonated through hydrolysis. To determine the RDS for TiO$_2$ and TiO$_2$/PEI photoanodes, we calculated the reaction orders (β) of solar water oxidation by the rate law analysis (Figure 5b,c). According to literature,[7,35,36,42] β values can be determined as a slope of the logarithmic graph between surface hole density and steady-state current—that were measured by EIS and chronoamperometry under various light intensities (Figures S22–S24, Supporting Information)—and provide the information about the number of charge carriers involved in RDS and reaction pathways. At pH 4.0, TiO$_2$ and TiO$_2$/PEI had the β values of ≈2 and ≈3, respectively, and the TiO$_2$/PEI photoanode had a larger β value at pH 4.0 than at pH 13.0 (≈3 vs 1.5). Interestingly, these results are partly in accordance with previous reports that most metal oxide photoanodes have larger β values at high pHs. For example, Kafizas et al.[43] also showed that TiO$_2$ requires two and three surface-trapped holes under acidic and basic conditions, respectively, to drive water–oxidation reaction due to different surface coverage of OH$^-$ near its surface that influences the RDS. In this respect, we anticipated that PEI hydrogel facilitates CPET and improves water oxidation kinetics by controlling the environment near the photoanode surface through the protonation of amine groups via hydrolysis. Confirmation of the local pH change by PEI hydrogel and the calculation of the electron-transfer coefficient also support our anticipation. We found that

the color of methyl orange, which is a well-known colorimetric pH indicator, immediately changed on PEI hydrogel-coated substrates due to the protonation of amine groups on PEI and the formation of OH$^-$ ions (Figure S25, Supporting Information). In addition, the bare TiO$_2$ had the transfer coefficients of 0.4 at pH 4.0 and 0.9 at pH 13. Of note, a smaller value under acidic conditions is known to be due to acidification near the (photo)electrode that led to sluggish water oxidation kinetics. In contrast, TiO$_2$/PEI had a larger electron-transfer coefficient at a lower pH of 4.0, suggesting that the PEI hydrogel increases the local OH$^-$ concentration more effectively at acidic pHs and alters the RDS (Figure 5d).[44,45]

2.4. Suggested Mechanism

Based on these results, we propose a mechanism for the enhanced PEC performance of various photoanodes by the PEI hydrogel (**Figure 6**).[35,36,42,43] First, PEI hydrogel could be protonated at the pH lower than the pKa values of the amine groups in PEI with concurrent deprotonation of water by photogenerated holes, forming the *OH intermediate. The protonated amine groups could stabilize the *OH intermediate and thereby reduce the activation energy for the transformation to *O intermediate.[46] This stabilizing process boost the first PCET process that is frequently regarded as RDS in
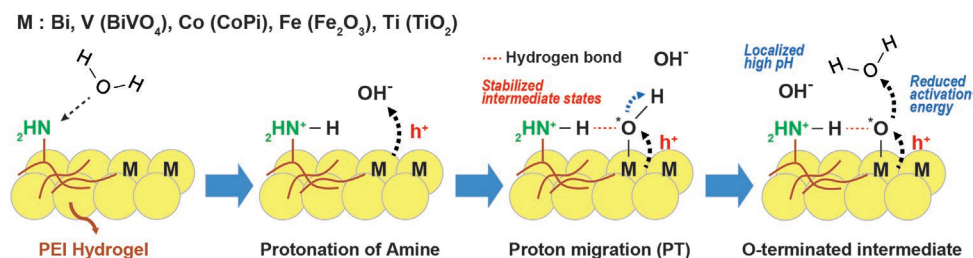
Figure 6. The proposed mechanism of PEI hydrogel for boosting charge transfer efficiency of photoanode. M indicates an active metal site in each metal oxide photoanode. Protonated amine group in PEI stabilized intermediate state of *OH, and increase of hydroxide ion near the electrode surface reduce activation energy in water-oxidation.

(photo)electrochemical water oxidation. Simultaneously, extra OH^- ions from the protonated amine could increase the locally high pH near the electrode surface and promote water oxidation process thermodynamically. On the other hand, negligible enhancement effect of the PEI layer at high pHs on the PEC performance can be explained by the presence of abundant OH^- ions even without PEI.

3. Conclusion

In summary, we report a facile and universally applicable method based on the modification of photoanodes with amine-rich PEI hydrogel to enhance their performance for solar water oxidation. Various photoanodes such as $BiVO_4$, Fe_2O_3, and TiO_2 exhibited significantly enhanced PEC water oxidation performance when modified with PEI hydrogel. We conducted systematic analyses, such as pH-dependent PEC performance, IPCE, EIS, OCP, and the reaction order measurements, to elucidate the role of PEI and the underlying mechanism for the enhanced PEC performance. Our results suggest that protonated amine groups of PEI hydrogel facilitate PEC water oxidation by promoting the PCET process and stabilizing the key intermediates, *OH and *O. We believe that our study can provide new insights into the design of novel (photo)electrochemical devices through hybridizing inorganic and organic materials.

4. Experimental Section

Materials: All chemicals were purchased from Sigma-Aldrich (St Louis, MO, USA) unless stated otherwise. Potassium iodide (KI) was obtained from Acros Organics (NJ, USA). Polyethylenimine (branched, $M_w \approx 25\,000$) including primary, secondary, and tertiary amine groups in ≈46/24/30 ratio was utilized for fabrication of hydrogel.

Fabrication of Nanoporous $BiVO_4$ Photoanodes: $BiVO_4$ was fabricated by electrodeposition as reported previously.[17,24] Briefly, 0.4 mol of KI was dissolved in 50 mL of deionized (DI) water, and the pH was adjusted to 1.7 using a 1 M HNO_3. The KI solution was then mixed with an ethanolic solution (20 mL) of 0.04 M of $Bi(NO_3)_3 \cdot 5H_2O$ and 0.23 M p-benzoquinone. Electrodeposition was carried out using fluorine-doped tin oxide (FTO), platinum coated FTO, and Ag/AgCl as the working, counter, and reference electrodes, respectively. BiOI was electrodeposited at −0.1 V versus Ag/AgCl for ≈5 min (total charge of 0.09 mA h cm^{-2} of FTO) and was washed with DI water. Subsequently, BiOI was covered with 0.15 mL of 0.13 M $VO(acac)_2$ in dimethyl sulfoxide and annealed at 450 °C for 2 h with a ramping rate of 2 K min^{-1}. After

annealing, the resulting $BiVO_4$ electrode was soaked in 1 M NaOH to remove excess V_2O_5 and dried with N_2.

Fabrication of Fe_2O_3 Photoanodes: Sn-doped Fe_2O_3 on FTO was synthesized according to literature.[14,15,25] Briefly, β-FeOOH nanowires were hydrothermally grown on FTO using a solution mixture of 0.15 M $FeCl_3 \cdot 6H_2O$ and 1.0 M $NaNO_3$ at 95 °C for 4 h. Sn-doped Fe_2O_3 photoanodes were prepared by two step annealing of β-FeOOH nanowires on FTO in air: 550 °C for 2 h (ramping rate of 4 K min^{-1}) and then 800 °C for 20 min.

Fabrication of TiO_2 Nanotube Photoanodes: TiO_2 nanotubes were fabricated by anodization of Ti foil as reported previously.[15,26] Briefly, NH_4F was dissolved at 0.3 wt% in a solution of 1 to 9 (w/w) mixture of DI water and ethylene glycol. Anodization was conducted at 60 V for 1 h in a two-electrode configuration using Ti foil and Pt plate as the working and counter electrodes, respectively. As-prepared samples were washed with DI water and ethanol thoroughly and annealed at 450 °C for 2 h (ramping rate of 2 K min^{-1}) to form TiO_2 nanotube photoanodes.

Photo-Assisted Electrodeposition of Cobalt Phosphate Co-Catalysts on $BiVO_4$: Cobalt phosphate (CoPi) co-catalyst was grown on $BiVO_4$ by photo-assisted electrodeposition methods.[19] A precursor solution of CoPi was prepared by dissolving $Co(NO_3)_2 \cdot 6H_2O$ at 0.15 mM in 0.1 M potassium phosphate buffer (pH 7.0). CoPi was electrodeposited on $BiVO_4$ at 0.3 V versus Ag/AgCl for 210 s under AM 1.5 G illumination.

Deposition of PEI Hydrogels on Photoanodes: PEI hydrogel was deposited on various photoanodes by spin-coating of PEI followed by crosslinking. PEI (branched, $M_w \approx 25\,000$) was dissolved at 10 wt% in DI water and spin-coated on the desired photoanode at 2000 rpm for 40 s and crosslinked using 2.5 vol% glutaraldehyde in 10 mM phosphate buffer solution with 137 mM NaCl (pH 5.0) to form a hydrogel for 5 min. As-prepared samples were washed with DI water to remove residual glutaraldehyde.

Characterizations: A Thermo Fisher K-alpha XPS spectrometer was used to investigate the elemental composition of various photoanodes. The morphology of photoanodes was examined using an S-4800 SEM (Hitachi High-Technologies, Japan) and a Tecnai TEM (Thermo Fisher, USA). SEM and TEM analyses were conducted at 5–10 and 200 kV, respectively. The pH-dependent zeta-potentials of PEI were measured with a Zetasizer nano-zs (Malvern, UK). Fourier-transform infrared (FT-IR) spectroscopy was conducted with a 670/620 spectrometer (Agilent, USA).

PEC Characterizations: PEC characterizations were carried out using an SP-150 potentiostat/galvanostat (BioLogic Science Instruments, France) in a three-electrode configuration using a photoanode, platinum deposited FTO, and Ag/AgCl as the working, counter, and reference electrodes, respectively. A Newport 94023A solar simulator (AAA class) and a 300 W Xe lamp with and without an AM 1.5 G filter were used as light sources for PEC measurements. Throughout PEC analysis, 0.5 M sodium sulfate was used as an electrolyte, and its pH was adjusted using H_2SO_4 and NaOH. The IPCE spectra were measured using a 300 W Xe lamp equipped with a CD130 monochromator (Newport Corporation, CA, USA) as a light source. OCP values were obtained under dark and light conditions. EIS was measured using a SP-150 potentiostat/galvanostat under various light intensity under the following conditions:

applied bias of 0.3 V (BiVO$_4$), 0.6 V (TiO$_2$), or 1.0 V (Fe$_2$O$_3$) versus RHE; amplitude of 20 mV; and frequency range from 0.1 Hz to 100 kHz. Numerical fitting of EIS data was carried out with an EC-Lab software (Bio-Logic Science Instruments, France).

Supporting Information

Supporting Information is available from the Wiley Online Library or from the author.

Conflict of Interest

The authors declare no conflict of interest.

Data Availability Statement

The data that support the findings of this study are available from the corresponding author upon reasonable request.

[1] S. Corby, R. R. Rao, L. Steier, J. R. Durrant, *Nat. Rev. Mater.* **2021**, *6*, 1136.

[2] W. Yang, R. R. Prabhakar, J. Tan, S. D. Tilley, J. Moon, *Chem. Soc. Rev.* **2019**, *48*, 4979.

[3] S. Bae, J. E. Jang, H. W. Lee, J. Ryu, *Eur. J. Inorg. Chem.* **2019**, *2019*, 2040.

[4] H. Li, H. Shang, Y. Shi, R. Yakimova, M. Syväjärvi, L. Zhang, J. Sun, *J. Mater. Chem. A* **2018**, *6*, 24358.

[5] J. Chen, Y. F. Li, P. Sit, A. Selloni, *J. Am. Chem. Soc.* **2013**, *135*, 18774.

[6] Y.-F. Li, Z.-P. Liu, L. Liu, W. Gao, *J. Am. Chem. Soc.* **2010**, *132*, 13008.

[7] Y. Zhang, H. Zhang, A. Liu, C. Chen, W. Song, J. Zhao, *J. Am. Chem. Soc.* **2018**, *140*, 3264.

[8] C. Pasquini, I. Zaharieva, D. Gonzalez-Flores, P. Chernev, M. R. Mohammadi, L. Guidoni, R. D. L. Smith, H. Dau, *J. Am. Chem. Soc.* **2019**, *141*, 2938.

[9] Y. Zhang, H. Zhang, H. Ji, W. Ma, C. Chen, J. Zhao, *J. Am. Chem. Soc.* **2016**, *138*, 2705.

[10] C. J. Gagliardi, A. K. Vannucci, J. J. Concepcion, Z. Chen, T. J. Meyer, *Energy Environ. Sci.* **2012**, *5*, 7704.

[11] J. W. Darcy, S. S. Kolmar, J. M. Mayer, *J. Am. Chem. Soc.* **2019**, *141*, 10777.

[12] Yang, H. J. M. de Groot, F. Buda, *ChemSusChem* **2021**, *14*, 479.

[13] D. Jeon, N. Kim, S. Bae, Y. Han, J. Ryu, *ACS Appl. Mater. Interfaces* **2018**, *10*, 8036.

[14] D. Jeon, H. Kim, C. Lee, Y. Han, M. Gu, B.-S. Kim, J. Ryu, *ACS Appl. Mater. Interfaces* **2017**, *9*, 40151.

[15] S. Bae, D. Kim, H. Kim, M. Gu, J. Ryu, B.-S. Kim, *Adv. Funct. Mater.* **2020**, *30*, 1908492.

[16] Y. Choi, S. Bae, B.-S. Kim, J. Ryu, *J. Mater. Chem. A* **2021**, *9*, 13874.

[17] T. W. Kim, K.-S. Choi, *Science* **2014**, *343*, 990.

[18] J. M. Yu, J. Lee, Y. S. Kim, J. Song, J. Oh, S. M. Lee, M. Jeong, Y. Kim, J. H. Kwak, S. Cho, C. Yang, J. W. Jang, *Nat. Commun.* **2020**, *11*, 5509.

[19] S. K. Pilli, T. E. Furtak, L. D. Brown, T. G. Deutsch, J. A. Turner, A. M. Herring, *Energy Environ. Sci.* **2011**, *4*, 5028.

[20] F. Malara, A. Minguzzi, M. Marelli, S. Morandi, R. Psaro, V. Dal Santo, A. Naldoni, *ACS Catal.* **2015**, *5*, 5292.

[21] R. Chong, G. Wang, Y. Du, Y. Jia, X. Wang, C. Li, Z. Chang, L. Zhang, *Chem. Eng. J.* **2019**, *366*, 523.

[22] B. Ni, K. Wang, T. He, Y. Gong, L. Gu, J. Zhuang, X. Wang, *Adv. Energy Mater.* **2018**, *8*, 1702313.

[23] S. Ye, C. Ding, R. Chen, F. Fan, P. Fu, H. Yin, X. Wang, Z. Wang, P. Du, C. Li, *J. Am. Chem. Soc.* **2018**, *140*, 3250.

[24] S. Bae, H. Kim, D. Jeon, J. Ryu, *ACS Appl. Mater. Interfaces* **2019**, *11*, 7990.

[25] J. Y. Kim, G. Magesh, D. H. Youn, J. W. Jang, J. Kubota, K. Domen, J. S. Lee, *Sci. Rep.* **2013**, *3*, 2681.

[26] L. Yu, Z. Wang, L. Zhang, H. B. Wu, X. W. Lou, *J. Mater. Chem. A* **2013**, *1*, 122.

[27] F. Lin, S. W. Boettcher, *Nat. Mater.* **2014**, *13*, 81.

[28] M. R. Nellist, J. Qiu, F. A. L. Laskowski, F. M. Toma, S. W. Boettcher, *ACS Energy Lett.* **2018**, *3*, 2286.

[29] Y. Shi, Y. Yu, Y. Yu, Y. Huang, B. Zhao, B. Zhang, *ACS Energy Lett.* **2018**, *3*, 1648.

[30] D. Jeon, J. Park, C. Shin, H. Kim, J.-W. Jang, D. W. Lee, J. Ryu, *Sci. Adv.* **2020**, *6*, 3944.

[31] M. Bae, Y. Kang, D. W. Lee, D. Jeon, J. Ryu, *Adv. Energy Mater.* **2022**, *12*, 2201452.

[32] J. Tan, B. Kang, K. Kim, D. Kang, H. Lee, S. Ma, G. Jang, H. Lee, J. Moon, *Nat. Energy* **2020**, *7*, 537.

[33] D. K. Lee, K.-S. Choi, *Nat. Energy* **2018**, *3*, 53.

[34] S. Zhang, M. Rohloff, O. Kasian, A. M. Mingers, K. J. J. Mayrhofer, A. Fischer, C. Scheu, S. Cherevko, *J. Phys. Chem. C* **2019**, *123*, 23410.

[35] Y. Zhang, Y. Zhang, W. Guo, A. C. Johnston-Peck, Y. Hu, X. Song, W. D. Wei, *Energy Environ. Sci.* **2020**, *13*, 1501.

[36] J. Li, W. Wan, C. A. Triana, H. Chen, Y. Zhao, C. K. Mavrokefalos, G. R. Patzke, *Nat. Commun.* **2021**, *12*, 255.

[37] T. Takashima, K. Hashimoto, R. Nakamura, *J. Am. Chem. Soc.* **2012**, *134*, 1519.

[38] Y. Nakabayashi, Y. Nosaka, *Phys. Chem. Chem. Phys.* **2015**, *17*, 30570.

[39] C. E. Gallops, C. Yu, J. D. Ziebarth, Y. Wang, *ACS Omega* **2019**, *4*, 7255.

[40] A. Sangiorgi, Z. Gonzalez, A. Ferrandez-Montero, J. Yus, A. J. Sanchez-Herencia, C. Galassi, A. Sanson, B. Ferrari, *J. Electrochem. Soc.* **2019**, *166*, H3239.

[41] W. Yang, T. Moehl, E. Service, S. D. Tilley, *Adv. Energy Mater.* **2021**, *11*, 2003569.

[42] C. A. Mesa, L. Francas, K. R. Yang, P. Garrido-Barros, E. Pastor, Y. Ma, A. Kafizas, T. E. Rosser, M. T. Mayer, E. Reisner, M. Gratzel, V. S. Batista, J. R. Durrant, *Nat. Chem.* **2020**, *12*, 82.

[43] A. Kafizas, Y. Ma, E. Pastor, S. R. Pendlebury, C. Mesa, L. Francàs, F. L.e Formal, N. Noor, M. Ling, C. Sotelo-Vazquez, C. J. Carmalt, I. P. Parkin, J. R. Durrant, *ACS Catal.* **2017**, *7*, 4896.

[44] S. Haghighat, J. M. Dawlaty, *J. Phys. Chem. C* **2015**, *119*, 6619.

[45] H. Cachet, E. M. M. Sutter, *J. Phys. Chem. C* **2015**, *119*, 25548.

[46] S. Zhang, P. Kang, S. Ubnoske, M. K. Brennaman, N. Song, R. L. House, J. T. Glass, T. J. Meyer, *J. Am. Chem. Soc.* **2014**, *136*, 7845.